

Efficient End-to-end Visual Localization for Autonomous Driving with Decoupled BEV Neural Matching

Jinyu Miao^{1,†}, Tuopu Wen^{1,†}, Ziang Luo¹, Kangan Qian¹, Zheng Fu¹, Yunlong Wang²,
Kun Jiang^{1,*}, Mengmeng Yang¹, Jin Huang¹, Zhihua Zhong³, Diange Yang^{1,*}

Abstract—Accurate localization plays an important role in high-level autonomous driving systems. Conventional map matching-based localization methods solve the poses by explicitly matching map elements with sensor observations, generally sensitive to perception noise, therefore requiring costly hyper-parameter tuning. In this paper, we propose an end-to-end localization neural network which directly estimates vehicle poses from surrounding images, without explicitly matching perception results with HD maps. To ensure efficiency and interpretability, a decoupled BEV neural matching-based pose solver is proposed, which estimates poses in a differentiable sampling-based matching module. Moreover, the sampling space is hugely reduced by decoupling the feature representation affected by each DoF of poses. The experimental results demonstrate that the proposed network is capable of performing decimeter level localization with mean absolute errors of 0.19m, 0.13m and 0.39° in longitudinal, lateral position and yaw angle while exhibiting a 68.8% reduction in inference memory usage.

I. INTRODUCTION

Visual localization serves as a vital component in high-level Autonomous Driving (AD) systems due to its ability to estimate vehicle poses with an economical sensor suite. In recent decades, several works have achieved extraordinary success in terms of localization accuracy and robustness [1].

A plethora of scene maps has been developed in the domain of visual localization research, yielding varying degrees of pose estimation accuracy [1]. In conventional robotic systems, visual localization systems often employ geo-tagged frames [2], [3] and visual landmark maps [4]. While economical mapping platforms can be utilized to construct such scene maps, their accuracy is often limited and the visual information is easily affected by visual conditions, resulting in unstable localization performance. Subsequently, some attempts have been made to perform visual localization using LiDAR point cloud maps [5]. The LiDAR map provides precise and stable 3D environmental

This work was supported in part by the National Natural Science Foundation of China (52394264, 52472449, U22A20104, 52372414, 52402499), Beijing Natural Science Foundation (23L10038, L231008), Beijing Municipal Science and Technology Commission (Z241100003524013, Z241100003524009), and China Postdoctoral Science Foundation (2024M761636).

[†]The authors contribute equally to this work.

¹Jinyu Miao, Tuopu Wen, Ziang Luo, Kangan Qian, Zheng Fu, Kun Jiang, Mengmeng Yang, Jin Huang, and Diange Yang are with the School of Vehicle and Mobility, Tsinghua University, Beijing, China. jinyu.miao97@gmail.com

²Yunlong Wang is with Autonomous Driving Division of NIO Inc., Beijing, China

³Zhihua Zhong is with Chinese Academy of Engineering, Beijing, China

*Corresponding author: Diange Yang and Kun Jiang

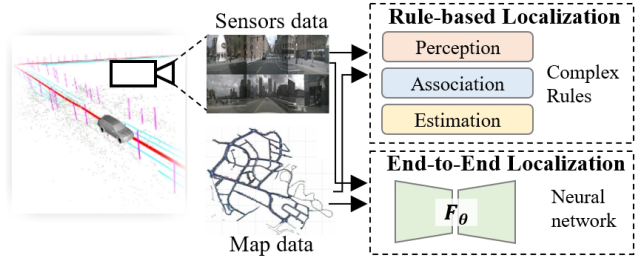


Fig. 1. The rule-based localization systems commonly involve perception, data association, and pose estimation, which contain plenty of complex hand-crafted rules, while end-to-end localization systems directly leverage a single neural network to estimate the vehicle pose.

information, but the visual sensor data and LiDAR point cloud belong to different modalities, which makes accurate data association and pose estimation technically challenging. Furthermore, these scene maps require huge storage space for unbounded scenarios. In AD society, High-Definition (HD) map, comprising vectorized semantic map elements [6], is a widely utilized representation format for static driving scenarios due to its significant compactness and accuracy. The HD map requires only approximately 50 KB/km of storage space, in comparison to around 600 MB/km for the raw LiDAR point cloud map [7]. Thus, HD maps are preferred by resource-limited intelligent vehicles.

Visual localization algorithms using HD map typically perform data association between perceived map elements and HD map elements, and then estimate the optimal pose based on the matched elements [1]. These solutions are contingent on precise data association, but the depth ambiguity inherent in visual cameras poses a technically challenging problem in terms of 2D-3D association between perception data and map data. Some studies project 3D HD map elements into 2D image planes [8], [9], [10], but the shapes of map elements differ from their original 3D shapes in the HD map due to the perspective effect of the camera model. Alternatively, there are methods that transform the perceived map elements into the Bird’s-Eye-View (BEV) space, following a common assumption that a vehicle is generally attached to the ground and its motion is constrained to 3 Degree-of-Freedom (DoF) [11], [12]. Traditional methods commonly utilize inverse projection mapping algorithms to facilitate view transformation, but their precision and stability are limited due to imprecise calibration and the unavoidable vibration of the camera [13]. In this work, we adopt the data association approach in BEV space, but we leverage

a learning-based view transformation technique to enhance performance and robustness. With regard to pose estimation, some methods utilize non-linear optimization-based solver [8], [7], [10], while Liao *et al.* proposed to use particle filter-based solver [9]. These traditional rule-based solutions have already achieved excellent performance in specific urban or highway scenes, but they all require hyperparameter and rule tuning based on trial-and-error, which hinders the wide deployment of visual localization systems.

In recent years, inspired by the achievements by End-to-End (E2E) systems in various areas, E2E visual localization algorithms have been proposed, as shown in Fig. 1. These methods employ learning-based neural networks to perceive the environment, align with the HD map, and subsequently estimate the pose, thereby circumventing the need for complex rules. Some methods initially develop E2E visual localization using Standard Definition (SD) map [14], [15], and only achieve meter-level localization accuracy due to the limited resolution of SD maps. Consequently, E2E visual localization methods using HD maps have been proposed, following a similar framework that first extracts BEV features from surrounding images and estimates poses by interacting BEV features with HD map data [16], [17]. By applying network learning on a vast amount of data, these E2E localization methods can achieve decimeter-level localization accuracy and great robustness against various environmental conditions. However, these methods either operate as a black-box [16] or require substantial computational resources [17]. Achieving an optimal balance among efficiency, interpretability, and localization accuracy remains a significant challenge for this emerging field.

To this end, in this paper, an E2E vehicle localization algorithm is developed, which combines learning-based BEV perception and differentiable pose estimation in a unified neural network. Specifically, the surrounding images and HD map data are first encoded into semantic BEV features, and then the optimal pose is estimated by aligning the two BEV features. A novel BEV neural matching-based pose solver is proposed in which we decouple the BEV representation affected by longitudinal, lateral positions, and yaw angle, so that we can solve these 3 DoF poses in a divide-and-conquer manner, thereby reducing sampling complexity in neural matching from cubic level to linear level. The primary contributions are summarized as follows.

- An E2E localization network is elaborated that performs fully differentiable and interpretable pose estimation using semantic BEV features perceived by surrounding cameras, achieving decimeter-level localization with lightweight HD maps.
- A decoupled BEV neural matching-based pose solver is proposed in the network to extract amplitude-frequency features and axis features to solve 3 DoF poses individually. This approach significantly reduces computational costs while achieving localization performance comparable to that of the traditional solution.
- Comprehensive experiments and detailed ablation analysis on public datasets are conducted to verify the

effectiveness of the proposed method.

II. RELATED WORKS

A. Learning-based Online HD Mapping

In recent years, the research community has increasingly adopted the BEV perception framework to construct HD map elements online, thereby reducing the substantial human effort typically required in conventional SLAM-based mapping pipelines. As a milestone, HDMaPNet [18] built the first online mapping and evaluation framework. It transforms image features into BEV features by a learnable neural network, fuses cross-modal features and directly learns map elements in BEV space. This framework has been extensively adopted in subsequent research [19], [20], [21]. SuperFusion [19] fuses visual and LiDAR data at multiple levels. P-MapNet [20] incorporates prior information from both the SD map and the HD map. DiffMap [21] introduces a diffusion module to learn the structural prior of HD map in this framework. These algorithms all tend to enhance the perceived BEV features through various methods. In contrast to these methods that rely on rasterized map predictions, VectorMapNet [22] directly estimates vectorized HD map elements through a Transformer architecture. Subsequently, BeMapNet [23] employs piecewise Bezier curves and achieves excellent perception performance. All of the aforementioned works construct online maps based on BEV features, paving the way for subsequent E2E localization.

B. Visual Localization based on HD Map

Traditional localization systems using vectorized HD map are contingent upon high-quality perception to extract semantic map elements (*e.g.*, lanes [24], poles [25], traffic signs [26], and their combinations [10]) from images. These methods then perform map matching with the HD map, thus overcoming the modal differences between sensor data and vectorized map elements. However, since HD map elements only possess shape and semantic information, repeated structures, missed and false detections, and inaccurate view transformations can render explicit data association highly ambiguous, thus posing a significant challenge to localization methods. Recently, researchers have begun to develop learning-based localization methods based on HD maps. As a beginning, BEVLocator [16] proposes an E2E localization network using surrounding images that it employs a full Transformer-based network to perform data association and pose estimation. It achieves $<20\text{cm}$ localization accuracy in longitudinal and lateral position, and it only requires single time surrounding images, as opposed to sequential images [10], [7]. Subsequently, EgoVM [17] enhances localization accuracy and interpretability by using more informative HD maps and a full template matching-based pose solver. Zhao *et al.* proposed to utilize BEV perception network to obtain BEV map elements and estimate pose by optimization-based solver [27]. These works all transform image features into BEV space and estimate pose based on BEV features and map features, which motivates our work. And we develop this in an E2E scheme.

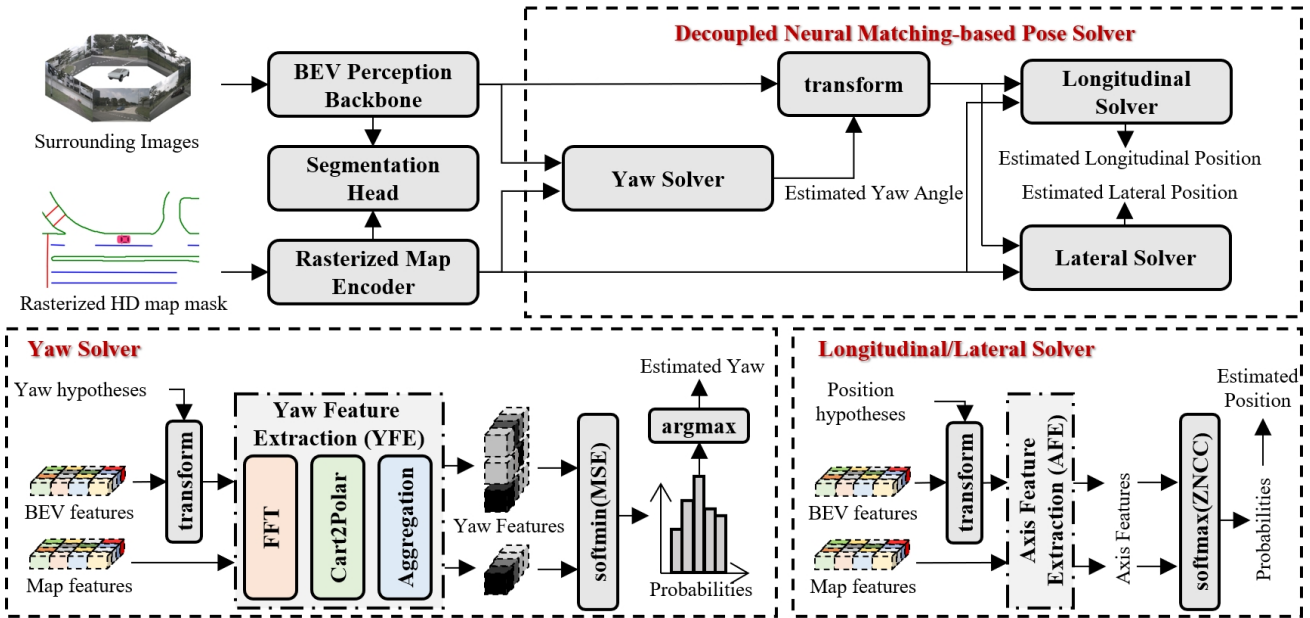


Fig. 2. An overview of the proposed end-to-end vehicle localization network, which contains BEV perception backbone, rasterized map encoder, and decoupled BEV neural matching-based pose solver.

III. METHODOLOGY

In this section, we first define the visual-to-HD map localization problem using surrounding cameras. Next, the overall framework of the proposed E2E localization network is presented. Then, we describe the three core modules in the network, *i.e.*, BEV perception backbone, map encoder, and decoupled neural matching-based pose solver in details.

A. Problem Formulation

Following a common assumption in AD area that the ground vehicle is attached to the flat ground, the ego pose in global frame can be degraded to 3 DoF in BEV space, *i.e.*, $\mathbf{T} = [x, y, \alpha] \in \mathbb{SE}(2)$, where x and y denote the longitudinal and lateral position, α is the heading/yaw angle. Given an initial vehicle pose \mathbf{T}_0 , the global HD map \mathcal{M} can be retrieved and cropped to a local HD map \mathcal{M}_0 . Therefore, the goal of visual-to-HD map localization task is to estimate an optimal camera pose $\Delta\hat{\mathbf{T}}$, which aligns the surrounding images $\{\mathbf{I}^i\}_{i=1}^V$ to the local HD map \mathcal{M}_0 :

$$\Delta\hat{\mathbf{T}} = \arg \min_{\Delta\mathbf{T}} d(\{\mathbf{I}^i\}_{i=1}^V, \text{transform}(\mathcal{M}_0, \Delta\mathbf{T})) \quad (1)$$

where $d(\cdot, \cdot)$ measures the differences between cross-modal data, and V is the number of surrounding camera. After that, the global ego pose can be obtained by $\hat{\mathbf{T}} = \mathbf{T}_0 \Delta\hat{\mathbf{T}}$.

B. Overview of the E2E Localization Network

To perform HD map-based localization in an E2E manner, the proposed method achieves both perception and localization in a unified network. As shown in Fig. 2, the network is fed by V surrounding images $\{\mathbf{I}^i\}_{i=1}^V$ and a local HD map \mathcal{M}_0 . The local HD map is represented by a rasterized semantic mask \mathbf{S} in BEV space by projection. We adopt a

BEV perception network as the backbone and obtain high-dimensional semantic features \mathbf{F}_B in BEV space. Meanwhile, we also convert \mathbf{S} into the map features \mathbf{F}_M by the map encoder network. Finally, the pose solver module is fed by \mathbf{F}_B and \mathbf{F}_M , and estimates an optimal pose $\Delta\hat{\mathbf{T}}$ by using the proposed decoupled BEV neural matching-based solver.

C. BEV Perception Backbone and Rasterized Map Encoder

Since the images and map data are in different modalities, precise cross-modal matching and pose estimation between them are technically challenging. In order to make cross-modal data matchable, we extract high-dimensional semantic BEV features from both surrounding images and map mask.

Inspired by recent success in online mapping works [18], [23], we employ a well-established BEV mapping network, BeMapNet [23], as the BEV perception backbone. The backbone takes a set of surrounding images $\{\mathbf{I}^i\}_{i=1}^V$, intrinsics $\{\mathbf{K}^i\}_{i=1}^V$ and extrinsics $\{\mathbf{E}^i\}_{i=1}^V$ of cameras as input, and extracts Perspective-View (PV) features from each image. Then, the backbone projects and aggregates PV features into BEV space by a Transformer-based view transformation module, and finally obtains BEV semantic features \mathbf{F}_B . We discard the instance decoder and original output head of BeMapNet [23], and add a simple segmentation head \mathcal{H} composed of two convolution layers to decode the BEV feature \mathbf{F}_B to semantic mask $\hat{\mathbf{S}}$ as in [18], [23]:

$$\mathbf{F}_B = \text{backbone}(\{\mathbf{I}^i, \mathbf{K}^i, \mathbf{E}^i\}_{i=1}^V), \quad \hat{\mathbf{S}} = \mathcal{H}(\mathbf{F}_B) \quad (2)$$

Meanwhile, we also build a VGG-like network [28] as the map encoder to extract high-dimensional map features \mathbf{F}_M from rasterized map mask \mathbf{S} , and also reconstruct the map mask by $\hat{\mathbf{S}}$ so that the map features should maintain

semantic and spatial information of the rasterized map.

$$\mathbf{F}_M = \text{encoder}(\mathbf{S}), \hat{\mathbf{S}} = \mathcal{H}(\mathbf{F}_M) \quad (3)$$

where $\hat{\mathbf{S}}$ is the reconstructed map mask.

By applying the backbone and the encoder, the surrounding images and map in different modalities are converted to matchable BEV semantic features $\mathbf{F}_B, \mathbf{F}_M$. To further reduce computational costs, we compress the size $H_c \times W_c$ and dimension C of both two BEV features through three residual blocks before feeding them into the pose solver.

D. Decoupled BEV Neural Matching-based Pose Solver

Preliminary: Full Neural Matching Traditional neural matching-based 3 DoF pose solver in BEV space exhaustively samples all possible pose hypotheses and then estimates their probabilities based on the feature similarities of BEV features transformed by pose hypotheses, which is widely utilized in radar odometry [29], map matching-based localization [17], and multi-modal sensor alignment [30]. Concretely, given two BEV features $\mathbf{F}_q, \mathbf{F}_r$, existing methods first sample pose hypotheses along the 3 DoF pose dimension (longitudinal position Δx , lateral position Δy , yaw angle $\Delta \alpha$) by grid sampling: $\{\Delta \mathbf{T}_{ijk} = [\Delta x_i, \Delta y_j, \Delta \alpha_k]\}$, where $i \in [1, N_x], j \in [1, N_y], k \in [1, N_\alpha]$ and N_x, N_y, N_α are the numbers of hypotheses sampled in each dimension. Then, \mathbf{F}_r is transformed based on the pose hypotheses:

$$\mathbf{F}_r^{ijk} = \text{transform}(\mathbf{F}_r, \Delta \mathbf{T}_{ijk}) \quad (4)$$

so that we obtain transformed BEV features corresponding to pose hypotheses, $\{\mathbf{F}_r^{ijk}\}$. Then, the probability of each hypothesis, $p(\Delta \mathbf{T}_{ijk})$, can be measured by normalized Zero-Normalized Cross Correlation (ZNCC) between \mathbf{F}_q and \mathbf{F}_r^{ijk} :

$$p(\Delta \mathbf{T}_{ijk}) = \text{softmax}(\text{ZNCC}(\mathbf{F}_q, \mathbf{F}_r^{ijk})) \quad (5)$$

Finally, the pose hypothesis with the highest probability is selected as the optimal estimation of the pose:

$$\Delta \hat{\mathbf{T}} = \Delta \mathbf{T}_{ijk}, \quad ijk = \arg \max_{ijk} p(\Delta \mathbf{T}_{ijk}) \quad (6)$$

In the full neural matching-based pose solver, we observe that the total number of pose hypotheses is as high as $N_x \times N_y \times N_\alpha$. This leads to an unacceptable computation burden in Eqn. 4-6 and slow convergence when the hypothesis space is extremely large. This hinders the practical use of the solver on resource-limited mobile platforms.

Decoupled Neural Matching Therefore, in this paper, we propose to decouple the feature representation affected by each DoF of poses and estimate each DoF of poses by decoupled neural matching in a divide-and-conquer framework. The proposed pose solver is implemented in a fully differentiable manner, allowing for E2E training along with the BEV perception backbone and the map encoder. As shown in Fig. 2, the proposed pose solver first extracts *yaw feature* from \mathbf{F}_B and \mathbf{F}_M and solves yaw angle by measuring differences between *yaw features*. Second, \mathbf{F}_B is transformed to \mathbf{F}_B^α by estimated yaw angle so that the \mathbf{F}_B^α and \mathbf{F}_M should only have differences in longitudinal and lateral positions.

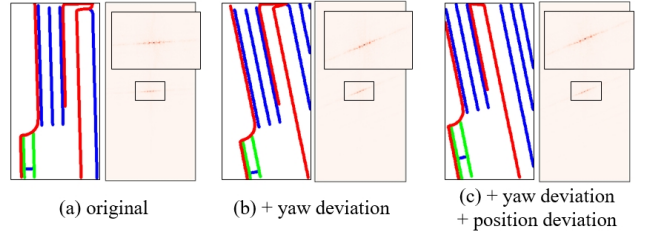


Fig. 3. Visualization cases of the amplitude-frequency feature for map mask. The left image in each group is HD map mask while the right one is its amplitude-frequency graph. (a) shows an original HD map, (b) shows a map after adding 10° yaw deviation, and (c) shows a map after adding 10° yaw deviation and 5m deviation in both longitudinal and lateral direction.

Finally, we extract *axis feature* from \mathbf{F}_B^α and \mathbf{F}_M and solve longitudinal and lateral positions. The decoupled pose solvers for yaw angle, longitudinal position, and lateral position will be individually introduced in details below.

Yaw Solver by Amplitude-Frequency Features As shown in Fig. 3, the amplitude-frequency graph of an image is only affected by its orientation but not its position [29], [31]. Inspired by such a character, we design a Yaw Feature Extraction (YFE) module in the yaw solver to decouple the BEV feature representation affected by yaw angle. Formally, we generate yaw hypotheses by grid searching:

$$\{\Delta \mathbf{T}_k^\alpha = [\Delta \alpha_k] | 1 \leq k \leq N_\alpha\} \quad (7)$$

Then, \mathbf{F}_B is transformed based on the yaw hypotheses and we get transformed BEV features $\{\mathbf{F}_B^{\alpha(k)} | 1 \leq k \leq N_\alpha\}$. The transformed BEV features and \mathbf{F}_M are fed into the YFE module to generate corresponding *yaw features* $\{\mathbf{Y}_B^{\alpha(k)} | 1 \leq k \leq N_\alpha\}$ and \mathbf{Y}_M . In the proposed YFE module, each feature is firstly converted into frequency domain by Fast Fourier Transformation (FFT) process so that we can obtain Frequency-BEV (F-BEV) features. Then, we transform the F-BEV features in Cartesian coordinates into polar F-BEV (PF-BEV) features in polar coordinates so that the amplitude-frequency features affected by yaw angle can be quantitatively represented in the yaw axis in polar coordinates. And we aggregate the PF-BEV features perpendicular to yaw axis (*i.e.*, radius axis) and generate *yaw features*:

$$\mathbf{Y}_* = \text{aggregate}(\text{Cart2Polar}(\text{FFT}(\mathbf{F}_*)) \quad (8)$$

The probability of each yaw hypothesis is calculated by normalized Mean Square Error (MSE) between *yaw features*:

$$p(\Delta \mathbf{T}_k^\alpha) = \text{softmax}(\text{MSE}(\mathbf{Y}_M, \mathbf{Y}_B^{\alpha(k)})) \quad (9)$$

and an optimal yaw angle can be estimated like Eqn. 6:

$$\Delta \hat{\alpha} = \Delta \alpha_k, \quad k = \arg \max_k p(\Delta \mathbf{T}_k^\alpha) \quad (10)$$

The estimated yaw angle is utilized to transform \mathbf{F}_B to correct the orientation differences between features.

Longitudinal/Lateral Solver by Axis Features As shown in Fig. 4, the position differences of features in longitudinal dimension can be quantitatively reflected in the row order of features. Therefore, to individually solve longitudinal and

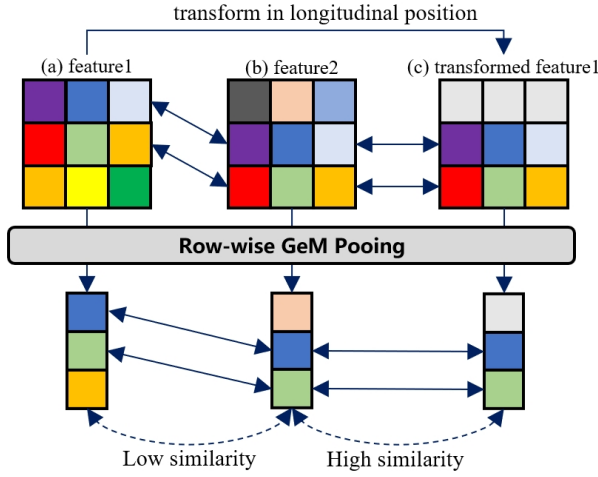


Fig. 4. A diagram of *axis feature* extraction by GeM pooling [32]. (a) and (b) show two features and their corresponding *axis features*. (c) shows a feature transformed from (a) in longitudinal dimension. Since the position differences of features in longitudinal dimension can be clearly represented in *axis features* after aggregation along the row dimension, the similarity between (b) and (c) is larger than the one between (a) and (b).

lateral positions, we propose to aggregate features along the single dimension by an Axis Feature Extraction (AFE) module so that the aggregated *axis features* differ only in the position of one dimension. For instance, to solve longitudinal position Δx , the longitudinal solver samples longitudinal hypotheses by grid sampling:

$$\{\Delta \mathbf{T}_i^x = [\Delta x_i] | 1 \leq i \leq N_x\} \quad (11)$$

Then, \mathbf{F}_B^α is transformed based on longitudinal hypotheses and we get transformed BEV features $\{\mathbf{F}_B^{x(i)} | 1 \leq i \leq N_x\}$. The transformed BEV features and map feature are fed into the AFE module. In the AFE module, each feature $\mathbf{F} \in \mathbb{R}^{H_c \times W_c \times C}$ is aggregated by GeM pooling [32] along the single row dimension and generate *axis feature* $\mathbf{A} \in \mathbb{R}^{H_c \times C}$:

$$\mathbf{A}[u] = \left(\frac{1}{W_c} \sum_{v=1}^{W_c} (\mathbf{F}[u, v])^\omega \right)^{1/\omega} \quad (12)$$

where u, v are the row and column index, ω is the weighting factor. Then, the probability of each longitudinal hypothesis is the normalized ZNCC between *axis features*:

$$p(\Delta \mathbf{T}_i^x) = \text{softmax}(\text{ZNCC}(\mathbf{A}_M, \mathbf{A}_B^{x(i)})) \quad (13)$$

and an optimal longitudinal position is estimated as in Eqn. 10. The lateral solver performs in a technically similar way but it aggregates features along the single column dimension.

E. Training Scheme

In order to make sure a stable and fast convergence of network training, we conduct a two-stage training scheme. In the first stage, we load the pre-trained BeMapNet weights [23] and finetune the BEV perception backbone and the rasterized map encoder with semantic supervision \mathcal{L}_{sem} [23] on both $\tilde{\mathbf{S}}$ and $\hat{\mathbf{S}}$. This stage ensures that the BEV features

and the map features contains implicit semantic map element information, which are matchable for the pose solver.

Then, in the second stage, we further add pose supervision \mathcal{L}_{pose} for E2E network training. We generate training and validation dataset as in [16]. We add random noises on real vehicle poses with longitudinal deviation Δx , lateral deviation Δy , and yaw deviation $\Delta \alpha$. The HD maps \mathcal{M} are transformed and cropped by this noised vehicle poses, and fed into the proposed network as \mathcal{M}_0 . Therefore, the task of the localization network is to predict the added pose deviations ($\Delta \mathbf{T}^* = [\Delta x, \Delta y, \Delta \alpha]$) from \mathcal{M}_0 and the surrounding images. Therefore, $\Delta \mathbf{T}^*$ can act as the supervision, allowing the network to be trained in an E2E manner. The proposed decoupled neural matching-based pose solver provides the probability distribution of 3 DoF pose hypotheses, $\mathbf{P}_x = \{p(\Delta \mathbf{T}_i^x)\}_{i=1}^{N_x}$, $\mathbf{P}_y = \{p(\Delta \mathbf{T}_j^y)\}_{j=1}^{N_y}$, $\mathbf{P}_\alpha = \{p(\Delta \mathbf{T}_k^\alpha)\}_{k=1}^{N_\alpha}$. Generally, we hope the pose hypotheses near the ground-truth pose $\Delta \mathbf{T}^*$ have higher probabilities while decreasing the probabilities of other pose hypotheses. So, we directly add pose supervisions \mathcal{L}_{pose} on the probability distributions of 3 DoF pose hypotheses. For example, we sample the probability of ground-truth yaw deviation $\Delta \alpha$ from the probability distribution of yaw hypotheses \mathbf{P}_α , and calculate its negative logarithmic value:

$$\mathcal{L}_{pose}(\Delta \alpha) = -\log(\text{sample1d}(\mathbf{P}_\alpha, \Delta \alpha)) \quad (14)$$

As the loss decreases, the probability of $\Delta \alpha$ will increase. The pose losses for longitudinal and lateral positions are similar to the yaw angle. Therefore, the final loss utilized in the second E2E training stage is:

$$\mathcal{L} = \mathcal{L}_{sem}(\tilde{\mathbf{S}}) + \mathcal{L}_{sem}(\hat{\mathbf{S}}) + 0.1 \cdot (\mathcal{L}_{pose}(\Delta x) + \mathcal{L}_{pose}(\Delta y) + \mathcal{L}_{pose}(\Delta \alpha)) \quad (15)$$

IV. EXPERIMENTS

A. Implementation Details

Model: We implemented the proposed network using PyTorch library. The proposed network is trained using AdamW optimizer, a batch size of 8, an initial learning rate of $1e^{-4}$, a weighting decay rate of $1e^{-7}$ on 4 Tesla V100 GPU. The first stage is trained for 20 epochs and the second stage train the whole model for another 15 epochs. We follow the same configuration of BeMapNet [23] that the BEV perception focus on three kinds of static map elements, *i.e.*, lane divider, pedestrian crossing, and road boundary. The perception ranges are $[-15.0m, 15.0m]$ for the lateral dimension and $[-30.0m, 30.0m]$ for the longitudinal dimension. And the resolution of BEV grid is set as 0.15m/pixel, generating 400×200 rasterized HD map masks. The sampling ranges of pose hypotheses are set to $\pm 2m$, $\pm 1m$, $\pm 2^\circ$ in longitudinal, lateral, and yaw dimension, and the sampling steps are set to 0.2m, 0.2m and 0.2° if not specific. Therefore, the amounts of pose hypotheses in each dimension are 21, 11, and 21, respectively. The features fed into the pose solver are compressed to $H_c \times W_c = 100 \times 50$ and $C = 16$ by default for efficiency, and the model can run in approximately 16.17 ms on a Tesla V100 GPU.

TABLE I

COMPARISON OF LOCALIZATION ACCURACY WITH EXISTING METHODS IN TERMS OF LONGITUDINAL, LATERAL AND YAW ERRORS.

Methods	Sensors	Dataset	localization error ↓		
			x (m)	y (m)	α (°)
Measured by Root Mean Square Error (RMSE)					
Pauls et al. [34]	mono.	Karlsruhe	0.86	0.23	0.58
		Ludwigsburg	0.90	0.11	0.56
Xiao et al. [8]	mono.	scenario 1	0.27	-	-
		scenario 2	0.37	-	-
Xiao et al. [7]	mono.	scenario 1	0.21	-	-
		scenario 2	0.29	-	-
Zhao <i>et al.</i> [27]	surro.	nuScenes	0.34	-	-
ICP [27]	surro.	nuScenes	0.39	-	-
ours (Full)	surro.	nuScenes	0.45	0.26	0.59
ours (Dec.)	surro.	nuScenes	0.37	0.21	0.59
Measured by Mean Absolute Error (MAE)					
Pauls et al. [34]	mono.	Karlsruhe	0.70	0.19	0.45
		Ludwigsburg	0.73	0.07	0.28
Wang et al. [35]	mono.	urban	0.43	0.12	0.11
BEVLocator [16]	surro.	nuScenes	0.18	0.08	0.51
ours (Full)	surro.	nuScenes	0.26	0.15	0.37
ours (Dec.)	surro.	nuScenes	0.19	0.13	0.39

“mono.” is monocular camera while “surro.” is 6 surrounding cameras.

Benchmark: The nuScenes dataset [33] is utilized in this paper, which consist of 28,130/6,019 samples and 700/150 driving scenes for the training/validation, respectively. Only 6 surrounding cameras are used in the visual localization task. As in Sec. III-E, during the training and validation process, we add random pose deviations to real vehicle poses as the initial vehicle pose. The ranges of randomly generated longitudinal, lateral, and yaw deviation are set to $\pm 2m$, $\pm 1m$, $\pm 2^\circ$. We measure the localization accuracy of estimated 3 DoF poses [16], and Intersection-over-Union (IoU) scores of perceived static map elements [18] for quantitative evaluation and comparison.

B. Comparison with the State-of-the-Arts

To prove the effectiveness of the proposed E2E localization network, we evaluate the localization accuracy in terms of the estimated 3 DoF poses on nuScenes dataset [33]. And we compare our methods with existing rule-based visual localization methods [34], [8], [7], [35], [27] and learning-based method [16]. For fairness, we report the used datasets and metrics of compared methods, since some methods are tested on self-collected data and evaluated using Root Mean Square Error (RMSE) or Mean Absolute Error (MAE). We also test the performance of the E2E localization network with full BEV neural matching-based (“ours (Full)”) and decoupled BEV neural matching-based pose solver (“ours (Dec.)”), as listed in Tab. I.

The table shows that our proposed method **ours (Dec.)** can achieve decimeter-level accuracy with MAE of 0.19m

TABLE II

ONLINE PERCEPTION PERFORMANCE OF OUR METHOD.

Methods	IoU scores (%)		
	Lane Divider	Pedestrian Crossing	Road Boundary
ours	57.8	42.2	57.8

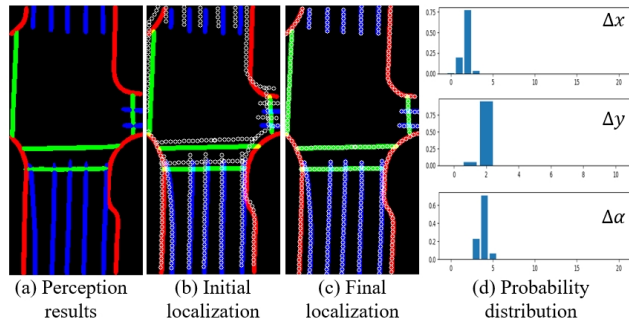


Fig. 5. An example that the proposed method achieves localization with a MAE of 0.03m, 0.04m, 0.18° . (a) shows the perception results, (b) illustrates the map projection using initial pose, (c) displays the map projection using estimated pose, (d) presents the estimated probability distribution of the 3 DoF poses. In (b) and (c), the projected HD map points are drawn in white circles, while the ground-truth HD map mask is drawn in blue, green, red lines, corresponding to lane dividers, pedestrian crossings, and road boundaries, respectively.

in longitudinal position, 0.13m in lateral position, and 0.39° in yaw angle on a challenging dataset, indicating the effectiveness of the proposed method. Compared to the method proposed by Zhao *et al.* [27], we also perform BEV perception, but we estimate pose in an E2E scheme through deep neural networks and differentiable calculation processes, so the parameters of pose solver network can be automatically tuned throughout the training stage, leading to better robustness and localization accuracy. BEVLocator [16] achieves better performance in lateral pose estimation, which is probably benefit from its utilized vectorized HD map information but not rasterized HD map mask. But it runs as an unexplainable black-box and its performance on yaw angle estimation is limited. Compared to those rule-based algorithms using monocular camera [34], [8], [7], [35], the proposed method achieves better performance even in a more challenging dataset with various visual conditions, showing the great advantages and potentials of the E2E methods.

Our E2E method perceives static map elements while estimating vehicle pose, thus we also test the perception performance following [18], as listed in Tab. II. The results show that we can obtain high-quality BEV semantic features, which is reflected in the performance of online mapping. The features provide robust data support for downstream high-precision localization.

Additionally, we provide a visualization case in Fig. 5. Our method can jointly perceive the environment (see Fig. 5 (a)) and perform localization (see Fig. 5 (b-d)). By applying our method, the vehicle pose can be accurately estimated, so the final map projection can be precisely aligned with the

TABLE III

THE LOCALIZATION PERFORMANCE USING VARIOUS POSE SOLVER.

Solver	Input	C	MAE ↓			Inference Memory (MiB)
			x (m)	y (m)	α (°)	
Original	-	-	1.00	0.50	1.00	-
Full	F	16	0.31	0.14	0.35	9653.74
Dec.	S	4	0.68	0.25	0.70	3010.84
Dec.	F	16	0.27	0.14	0.40	3012.01
Dec.	F	64	0.19	0.13	0.38	3020.81

ground-truth map although the initial pose is far away from the real vehicle pose. Figure 5 (d) shows that the estimated probability distributions of 3 DoF pose from our method exhibit a trend towards a single peak near the ground-truth value, which helps to select the optimal pose based on its probability.

C. Ablation Analysis

To better understand the effectiveness of the proposed method and select the optimal configurations, we conduct detailed ablation studies through a series of experiments. For fast analysis, the models evaluated in this subsection are trained for only 5 epochs in the second E2E training stage.

1) *Effectiveness of decoupled BEV neural matching:* We compare the performance of the E2E localization networks with full BEV neural matching-based (“Full”) and decoupled BEV neural matching-based pose solver (“Dec.”). The results are listed in Tab. I (trained for 15 epochs) and Tab. III (trained for 5 epochs). It can be seen that Dec. significantly reduces the computational costs compared to Full, from 9653.74 MB to 3012.01 MB (decreasing by about 68.8%), using the same inputs ($C = 16$), while achieving comparable or even better localization accuracy. Theoretically, the amount of samples in Full is $21 \times 11 \times 21 = 4,851$ whereas for Dec., it is $21 + 11 + 21 = 53$, which is decreasing about 98.9%, leading to a significant improvement in the computational efficiency of the proposed method.

2) *Effectiveness of BEV features:* We test the performance of the proposed pose solvers with different inputs. As shown in Tab. III, when feeding perception results $\tilde{\mathbf{S}}$ and reconstructed map mask $\hat{\mathbf{S}}$ into the pose solver, the localization accuracy will be declined significantly compared to that with BEV features $\mathbf{F}_B, \mathbf{F}_M$ as inputs. It indicates that high-dimensional features are more informative and representative than semantic map elements, thus promoting the data association in pose estimation. As the feature dimension increases, the localization accuracy will be improved, but resulting in enlarged computational costs. To maintain a balance between efficiency and performance, we set $C = 16$ as default configuration.

3) *Effectiveness of BEV size:* We also evaluate the effect of the BEV size of compressed BEV features and map features on the localization performance. We test a variant using features of enlarged size ($H_c \times W_c = 400 \times 200$), and

TABLE IV

THE LOCALIZATION PERFORMANCE USING DECOUPLED BEV NEURAL MATCHING-BASED POSE SOLVER WITH VARIOUS CONFIGURATIONS.

BEV size	step	MAE ↓			Inference Memory (MiB)
		x (m)	y (m)	α (°)	
original	-	1.00	0.50	1.00	-
100×50	0.1	0.26	0.13	0.40	3013.35
100×50	0.2	0.27	0.14	0.40	3012.01
100×50	0.4	0.26	0.16	0.40	3011.06
400×200	0.1	0.16	0.14	0.35	3080.18
400×200	0.2	0.16	0.13	0.35	3041.28
400×200	0.4	0.22	0.16	0.36	3028.57

the results are listed in Tab. IV. It can be seen that enlarging the feature size can consistently boost localization accuracy, but it also increases computational burden. Larger features in BEV space provide more detailed information, which helps the model align the perceived features with the map features.

4) *Effectiveness of sampling step:* The BEV neural matching generates pose hypotheses by grid sampling, so we test the effect of the sampling step in each DoF of poses on the localization performance, as shown in Tab. IV. When using features with limited size, refining the sampling step does not lead to significant improvements in the performance of neural matching. But if we increase the size of used features, refining the sampling step could effectively improve the localization performance. In this work, the BEV grid is set to 0.15m/pixel, so the proposed methods generally achieve similar capabilities when the sampling step is set to 0.1 or 0.2.

V. CONCLUSIONS

In this paper, we address the visual-to-HD map localization problem by proposing an E2E localization network using a novel decoupled BEV neural matching-based pose solver, which ensures interpretability and computational efficiency while achieving decimeter-level localization accuracy. The network extracts high-dimensional semantic BEV features and map features through a well-established BEV perception backbone and a rasterized map encoder, which overcomes the modality difference between visual images and vectorized HD map data. Then, both two features are fed into the decoupled BEV neural matching-based pose solver, in which the BEV representations affected by longitudinal, lateral positions, and yaw angle are decoupled, allowing us to solve the 3 DoF pose individually in a divide-and-conquer manner. The proposed network is fully analyzed on the nuScenes dataset [33] and is concluded to be able to achieve high-precision localization with a MAE of 0.19m, 0.13m, and 0.39° in longitudinal, lateral positions, and yaw angle. And it significantly reduces the number of samples from $N_x \times N_y \times N_\alpha$ to $N_x + N_y + N_\alpha$, resulting in an inference memory savings of up to 68.8% compared to traditional full BEV

neural matching, which is essential for accurate and efficient pose estimation for high-level autonomous driving.

REFERENCES

- [1] J. Miao, K. Jiang, T. Wen, Y. Wang, P. Jia, B. Wijaya, X. Zhao, Q. Cheng, Z. Xiao, J. Huang, *et al.*, “A survey on monocular re-localization: From the perspective of scene map representation,” *IEEE Transactions on Intelligent Vehicles*, 2024.
- [2] A. Ali-bey, B. Chaib-draa, and P. Giguère, “Boq: A place is worth a bag of learnable queries,” in *Proceedings of 2024 IEEE/CVF Conference on Computer Vision and Pattern Recognition (CVPR)*, 2024, pp. 17 794–17 803.
- [3] H. Yue, J. Miao, W. Chen, W. Wang, F. Guo, and Z. Li, “Automatic vocabulary and graph verification for accurate loop closure detection,” *Journal of Field Robotics*, vol. 39, no. 7, pp. 1069–1084, 2022.
- [4] P.-E. Sarlin, C. Cadena, R. Siegwart, and M. Dymczyk, “From coarse to fine: Robust hierarchical localization at large scale,” in *Proceedings of the IEEE/CVF conference on computer vision and pattern recognition (CVPR)*, 2019, pp. 12 716–12 725.
- [5] J. Miao, K. Jiang, Y. Wang, T. Wen, Z. Xiao, Z. Fu, M. Yang, M. Liu, J. Huang, Z. Zhong, *et al.*, “Poses as queries: End-to-end image-to-lidar map localization with transformers,” *IEEE Robotics and Automation Letters*, vol. 9, no. 1, pp. 803–810, 2023.
- [6] R. Liu, J. Wang, and B. Zhang, “High definition map for automated driving: Overview and analysis,” *The Journal of Navigation*, vol. 73, no. 2, pp. 324–341, 2020.
- [7] Z. Xiao, D. Yang, T. Wen, K. Jiang, and R. Yan, “Monocular localization with vector hd map (mlvhm): A low-cost method for commercial ivs,” *Sensors*, vol. 20, no. 7, p. 1870, 2020.
- [8] Z. Xiao, K. Jiang, S. Xie, T. Wen, C. Yu, and D. Yang, “Monocular vehicle self-localization method based on compact semantic map,” in *Proceedings of 2018 21st International Conference on Intelligent Transportation Systems (ITSC)*. IEEE, 2018, pp. 3083–3090.
- [9] Z. Liao, J. Shi, X. Qi, X. Zhang, W. Wang, Y. He, X. Liu, and R. Wei, “Coarse-to-fine visual localization using semantic compact map,” in *Proceedings of 2020 3rd International Conference on Control and Robots (ICCR)*. IEEE, 2020, pp. 30–37.
- [10] T. Wen, K. Jiang, B. Wijaya, H. Li, M. Yang, and D. Yang, “Tm3loc: Tightly-coupled monocular map matching for high precision vehicle localization,” *IEEE Transactions on Intelligent Transportation Systems*, vol. 23, no. 11, pp. 20 268–20 281, 2022.
- [11] R. P. D. Vivacqua, M. Bertozzi, P. Cerri, F. N. Martins, and R. F. Vassallo, “Self-localization based on visual lane marking maps: An accurate low-cost approach for autonomous driving,” *IEEE Transactions on Intelligent Transportation Systems*, vol. 19, no. 2, pp. 582–597, 2017.
- [12] L. Deng, M. Yang, B. Hu, T. Li, H. Li, and C. Wang, “Semantic segmentation-based lane-level localization using around view monitoring system,” *IEEE Sensors Journal*, vol. 19, no. 21, pp. 10 077–10 086, 2019.
- [13] W. Jang, J. Hyun, J. An, M. Cho, and E. Kim, “A lane-level road marking map using a monocular camera,” *IEEE/CAA Journal of Automatica Sinica*, vol. 9, no. 1, pp. 187–204, 2021.
- [14] A. B. Camilletto, A. Bochicchio, A. Liniger, D. Dai, and A. Gawel, “U-bev: Height-aware bird’s-eye-view segmentation and neural map-based relocalization,” in *Proceedings of 2024 IEEE/RSJ International Conference on Intelligent Robots and Systems (IROS)*. IEEE, 2024, pp. 5597–5604.
- [15] H. Wu, Z. Zhang, S. Lin, X. Mu, Q. Zhao, M. Yang, and T. Qin, “Maplocnet: Coarse-to-fine feature registration for visual re-localization in navigation maps,” in *Proceedings of 2024 IEEE/RSJ International Conference on Intelligent Robots and Systems (IROS)*. IEEE, 2024, pp. 13 198–13 205.
- [16] Z. ZHANG, M. XU, W. ZHOU, T. PENG, L. LI, and S. POSLAD, “Bev-locator: an end-to-end visual semantic localization network using multi-view images,” *SCIENCE CHINA Information Sciences*, vol. 68, no. 2, pp. 122 106–, 2025.
- [17] Y. He, S. Liang, X. Rui, C. Cai, and G. Wan, “Egovm: Achieving precise ego-localization using lightweight vectorized maps,” in *Proceedings of 2024 IEEE/RSJ International Conference on Intelligent Robots and Systems (IROS)*. IEEE, 2024, pp. 12 248–12 255.
- [18] Q. Li, Y. Wang, Y. Wang, and H. Zhao, “Hdmapnet: An online hd map construction and evaluation framework,” in *Proceedings of 2022 International Conference on Robotics and Automation (ICRA)*, 2022, pp. 4628–4634.
- [19] H. Dong, W. Gu, X. Zhang, J. Xu, R. Ai, H. Lu, J. Kannala, and X. Chen, “Superfusion: Multilevel lidar-camera fusion for long-range hd map generation,” in *Proceedings of 2024 IEEE International Conference on Robotics and Automation (ICRA)*. IEEE, 2024, pp. 9056–9062.
- [20] Z. Jiang, Z. Zhu, P. Li, H.-a. Gao, T. Yuan, Y. Shi, H. Zhao, and H. Zhao, “P-mapnet: Far-seeing map generator enhanced by both sdmap and hdmap priors,” *IEEE Robotics and Automation Letters*, 2024.
- [21] P. Jia, T. Wen, Z. Luo, M. Yang, K. Jiang, Z. Liu, X. Tang, Z. Lei, L. Cui, B. Zhang, *et al.*, “Diffmap: Enhancing map segmentation with map prior using diffusion model,” *IEEE Robotics and Automation Letters*, 2024.
- [22] Y. Liu, T. Yuan, Y. Wang, Y. Wang, and H. Zhao, “Vectormapnet: End-to-end vectorized hd map learning,” in *Proceedings of International Conference on Machine Learning (ICML)*. PMLR, 2023, pp. 22 352–22 369.
- [23] L. Qiao, W. Ding, X. Qiu, and C. Zhang, “End-to-end vectorized hd-map construction with piecewise bézier curve,” in *Proceedings of 2023 IEEE/CVF Conference on Computer Vision and Pattern Recognition (CVPR)*, 2023, pp. 13 218–13 228.
- [24] O. Pink, “Visual map matching and localization using a global feature map,” in *Proceedings of 2008 IEEE computer society conference on computer vision and pattern recognition workshops (CVPRW)*. IEEE, 2008, pp. 1–7.
- [25] R. Spangenberg, D. Goehring, and R. Rojas, “Pole-based localization for autonomous vehicles in urban scenarios,” in *Proceedings of 2016 IEEE/RSJ international conference on intelligent robots and systems (IROS)*. IEEE, 2016, pp. 2161–2166.
- [26] X. Qu, B. Soheilian, and N. Paparoditis, “Vehicle localization using mono-camera and geo-referenced traffic signs,” in *Proceedings of 2015 IEEE Intelligent Vehicles Symposium (IV)*. IEEE, 2015, pp. 605–610.
- [27] L. Zhao, Z. Liu, Q. Yin, L. Yang, and M. Guo, “Towards robust visual localization using multi-view images and hd vector map,” in *Proceedings of 2024 IEEE International Conference on Image Processing (ICIP)*, 2024, pp. 814–820.
- [28] K. Simonyan and A. Zisserman, “Very deep convolutional networks for large-scale image recognition,” in *Proceedings of 3rd International Conference on Learning Representations (ICLR)*, 2015.
- [29] R. Weston, M. Gadd, D. De Martini, P. Newman, and I. Posner, “Fastmbym: Leveraging translational invariance of the fourier transform for efficient and accurate radar odometry,” in *Proceedings of 2022 International Conference on Robotics and Automation (ICRA)*. IEEE, 2022, pp. 2186–2192.
- [30] M. Hosseinzadeh and I. Reid, “Bevpose: Unveiling scene semantics through pose-guided multi-modal bev alignment,” in *Proceedings of 2024 IEEE/RSJ International Conference on Intelligent Robots and Systems (IROS)*, 2024, pp. 14 111–14 118.
- [31] Y. Fan, X. Du, L. Luo, and J. Shen, “Fresco: Frequency-domain scan context for lidar-based place recognition with translation and rotation invariance,” in *Proceedings of 2022 17th International Conference on Control, Automation, Robotics and Vision (ICARCV)*, 2022, pp. 576–583.
- [32] F. Radenović, G. Toliás, and O. Chum, “Fine-tuning cnn image retrieval with no human annotation,” *IEEE Transactions on Pattern Analysis and Machine Intelligence*, vol. 41, no. 7, pp. 1655–1668, 2019.
- [33] H. Caesar, V. Bankiti, A. H. Lang, S. Vora, V. E. Liong, Q. Xu, A. Krishnan, Y. Pan, G. Baldan, and O. Beijbom, “nusscenes: A multimodal dataset for autonomous driving,” in *Proceedings of the IEEE/CVF conference on computer vision and pattern recognition (CVPR)*, 2020, pp. 11 621–11 631.
- [34] J.-H. Pauls, K. Petek, F. Poggenhans, and C. Stiller, “Monocular localization in hd maps by combining semantic segmentation and distance transform,” in *Proceedings of 2020 IEEE/RSJ International Conference on Intelligent Robots and Systems (IROS)*. IEEE, 2020, pp. 4595–4601.
- [35] H. Wang, C. Xue, Y. Zhou, F. Wen, and H. Zhang, “Visual semantic localization based on hd map for autonomous vehicles in urban scenarios,” in *Proceedings of 2021 IEEE International conference on robotics and automation (ICRA)*. IEEE, 2021, pp. 11 255–11 261.